Journal of Pharmaceutical Sciences 110 (2021) 2955–2965

Contents lists available at ScienceDirect

Journal of Pharmaceutical Sciences

journal homepage: www.jpharmsci.org

Pharmaceutics, Drug Delivery and Pharmaceutical Technology

Amelioration of Tumor Targeting and *In Vivo* Biodistribution of ^{99m}Tc-Methotrexate-Gold Nanoparticles (^{99m}Tc-Mex-AuNPs)

DM El-Safoury[a], Ahmed Badr Ibrahim[a,b,*], DA El-Setouhy[c], OM Khowessah[c], MA Motaleb[a], Tamer M. Sakr[b,d,*]

[a] *Labeled Compounds Department, Hot Labs Center, Egyptian Atomic Energy Authority, Cairo 13759, Egypt*
[b] *Radioisotopes Production Facility, Second Egyptian Research Reactor Complex, Egyptian Atomic Energy Authority, Cairo 13759, Egypt*
[c] *Pharmaceutics and Industrial Pharmacy Department, Faculty of Pharmacy, Cairo University, Cairo 11562, Egypt*
[d] *Radioactive Isotopes and Generator Department, Hot Labs Center, Egyptian Atomic Energy Authority, Cairo 13759, Egypt*

ARTICLE INFO

Article history:
Received 20 January 2021
Revised 25 March 2021
Accepted 25 March 2021
Available online 2 April 2021

Keywords:
Gold nanoparticles
^{99m}Tc-Methotrexate
In vitro characterization
In vitro cytotoxicity, ^{99m}Tc-Mex-AuNPs
In vivo biodistribution
Tumor targeting

ABSTRACT

Gold nanoparticles (AuNPs) represent very attractive and promising drug delivery carriers due to their unique dimensions, adjustable surface functions, and controllable drug release. Therefore, AuNPs are used to overcome the limitations of conventional chemotherapy, for example methotrexate (Mex), one of the first-generation chemotherapy drugs for cancer treatment, whose usefulness has been restricted due to drug resistance and dose-dependent side effects. In the present study, the AuNPs drug delivery system was synthesized and loaded with technetium-99 m radiolabeled Methotrexate (^{99m}Tc-Mex) to produce new potential nanoradiopharmaceutical for tumor targeting and further imaging. The Methotrexate loaded gold nanoparticles (Mex-AuNPs) successfully prepared in small spherical particle size (20.3 nm), polydispersity index PDI (< 0.5) and a zeta potential (−17.6 mV) with loading efficiency% (93 ± 1.2%) of methotrexate at 30 min as an optimum stirring time and showed strong absorption peak for Mex-AuNPs at λ_{max}, 525 nm. The *in vitro* release profile of Mex-AuNPs showed high release percent of methotrexate at pH 5; the $Q_{0.5}$ h and Q_{8h} were 21.2 ± 1.5% and 92.9 ± 3.4%, respectively. The *in vitro* cytotoxicity was investigated at different concentrations (0.024–50 μl/100 μl) of Mex-AuNPs (1 mg/ml) against MCF-7 (Michigan Cancer Foundation-7) breast cancer cells by MTT (3-(4,5-dimethylthiazol-2-yl)-2,5-diphenyl tetrazolium bromide) assay technique. Mex-AuNPs showed higher anticancer activity with low inhibitory concentration (IC_{50} = 0.098 μl/100 μl) that was three times lower than the inhibitory concentration (IC_{50}) of methotrexate (IC_{50} = 0.3 μl/100 μl). ^{99m}Tc-Mex complex prepared by direct reduction method at maximum radiochemical yield (RCY)% ~ 98.3 ± 1.09 % was loaded in AuNPs to form ^{99m}Tc-Mex-AuNPs with loading efficiency% (93 ± 1.2 %) at 30 min of stirring time. ^{99m}Tc-Mex-AuNPs showed convenient *in vitro* stability in mice serum up to 24 h with RCY% > 90 %. The preclinical biodistribution studies of ^{99m}Tc-Mex-AuNPs were performed in 3 experimental groups A (intravenous (I.V.) injected normal mice), B and C (I.V. and intratumor (I.T.) injected tumor bearing mice, respectively). The ^{99m}Tc-Mex-AuNPs achieved highest tumor uptake (93 ± 0.39 %ID/g) and highest Target/NonTarget (T/NT) ratio (58.1 ± 0.91) with high Tumor/Blood (T/B) ratio (25.8 ± 0.11) at 10 min post I.T. injection and retained high tumor uptake (79 ± 0.65 %ID/g) up to 60 min post I.T. injection before escaping into blood stream. Consequently, ^{99m}Tc-Mex-AuNPs can be considered as new potential nanoradiopharmaceutical in tumor diagnosis.

Introduction

Cancer is one of the most fatal diseases in the world as it kills millions of people every year. It is the second leading cause of death among humans in the world, and thus it is one of the major health concerns of the 21st century.[1] The number of cancer deaths worldwide is expected to increase by about 12 million deaths in 2030. Therefore, developing effective means of early diagnosis, monitoring and treating cancer is a challenge.[2] Methotrexate (Mex) is considered as a chemotherapy treatment used to treat certain types of cancer of the breast, skin, head and neck, lung, certain types of lymphoma, and leukemia.[3] It is a folic acid analogue[4] competitively inhibits dihydrofolate reductase (DHFR), an enzyme that participates in the tetrahydrofolate synthesis, blocking the conversion of dihydrofolate to

* Corresponding authors at: Radioisotopes Production Facility, Second Egyptian Research Reactor Complex, Egyptian Atomic Energy Authority, Cairo 13759, Egypt.
E-mail addresses: Ahmed_Badr1981@yahoo.com (A.B. Ibrahim), Tamer_Sakr78@yahoo.com (T.M. Sakr).

https://doi.org/10.1016/j.xphs.2021.03.021
0022-3549/

tetrahydrofolate, interfering with the growth of certain cells of the body, especially cells that reproduce quickly, such as cancer cells, bone marrow cells, and skin cells.[5] Methotrexate (Mex) may cause severe side effects called "methotrexate fog" that may occur one day after receiving a dose of methotrexate.[6] The side effects associated with the therapeutic dose of Mex, resistance of cancer cell, rapid metabolism and low selectivity of tumor cells have limited its anticancer effect.[7,8] Radiopharmaceuticals have been used as non-invasive molecular imaging agents to detect and monitor cancer at early stages and thus improving prognosis and treatment.[9] Therefore, it was important to find a technology to deliver the targeted radiopharmaceuticals to diagnose cancer cells at early stage and to bring hope to the oncological research world. Nanotechnology application in drug delivery was used as a strategy that may improve therapeutic efficacy of chemotherapy and decrease its side effects.[10] Using an ideal nanocarrier would greatly reduce the dose of the drug and improve its absorption from the body so that the patient can take a lower dose with the same benefit.[11] Gold nanocarriers (AuNPs) are widely used as a drug delivery in biomedicine especially in the diagnosis and treatment of cancer due to their unique physical and chemical properties such as safety, relative stability and ease of preparation.[12] Also, their small size helps them to penetrate widely and precipitate at the tumor site.[13] Hybridization of methotrexate with gold nanoparticles presented a valuable contribution in increasing drug accumulation in cancer cells and thus enhancing its cytotoxic efficacy with low inhibitory concentration (IC_{50}) with cancer cells rich in folate receptors[14] and human placental cancer cell lines[7], thus greater therapeutic efficacy than free methotrexate.[15] In the last decade, many innovative nanoradiopharmaceuticals drugs have shown amazing features in nuclear imaging. The anticancer drugs were hybridized with radioactive isotopes and AuNPs to be used in tumor diagnosis as ^{125}I-cRGD-GNPs,[16] ^{99}Tc-GNPs-HYNIC-GGC peptide/mannose[17] and ^{99m}Tc-Dox-EGCG-AuNPs.[18] The hybridization of ^{99m}Tc-Mex as a radiopharmaceutical with AuNPs to form a new nanoradiopharmaceutical could help to achieve progress in tumor imaging. The aim of the present study was to develop a nanoradiopharmaceutical as a novel diagnostic probe for tumors. Gold nanocarriers prepared by citrate reduction method were loaded with ^{99m}Tc-Mex in maximum RCY% to produce ^{99m}Tc-Mex-AuNPs complex. *In vitro* characterization, *in vitro* stability and cytotoxicity study were performed, following up on this the *in vivo* biological distribution of ^{99m}Tc-Mex-AuNPs (A theranostic nanoradiopharmaceutical) in normal and solid tumor bearing mice following I.V. and I.T. injection was studied to evaluate its ability to target the solid tumor and its imaging efficacy via molecular imaging Single photon emission computed tomography (SPECT) technique.

Materials and Methods

Materials

Methotrexate ($C_{20}H_{22}N_8O_5$) and Hydrogen tetrachloroaurate ($HAuCl_4 \bullet 3H_2O$) were purchased from Sigma-Aldrich Company, USA. Human breast carcinoma cells (MCF-7) provided by tissue culture unit, Vacsera, Giza, Egypt. Dulbecco's Modified Eagle's Medium (DMEM) Fetal Bovine serum, L-glutamine ($C_5H_{10}N_2O_3$) and gentamicin ($C_{21}H_{43}N_5O_7$) were purchased from Lonza group, Basel, Switzerland. Dimethyl sulfoxide (DMSO), ($(CH_3)_2SO$) was purchased from Prolabo, France. Female Albino Swiss mice had Ehrlich Ascites Carcinoma cell was obtained from Egyptian National Cancer Institute (NCI) (Cairo University, Cairo, Egypt). All other analytical grade (chemicals and solutions) and Whatman paper No.1 for paper chromatography (PC) were purchased from Merck Company, Germany. Technetium 99 m was obtained in the form of pertechnetate elute ($^{99m}TcO_4^-$) from the ^{99}Mo / ^{99m}Tc generator that was manufactured in the Radioisotope Production Facility (RPF) of the Egyptian Atomic Energy Authority (EAEA).

Synthesis of Methotrexate Loaded Gold Nanoparticles (Mex-AuNPs)

Citrate reduction method or Turkevich method was employed in gold nanoparticles synthesis[19,20] using solution of 1% trisodium citrate (0.05 g $Na_3C_6H_5O_7$ in 50 ml of double dist. H_2O) and stock solution of ~ 3.0×10^{-3} M tetrachloroauric acid (0.1 g $HAuCl_4$ in 100 ml double dist. H_2O). A fresh solution of aquaregia (HNO_3/HCl) (*3:1 v/v*) was prepared using concentrated nitric and hydrochloric acids with volume ratio 3:1 respectively, and used to clean all used glassware, followed by washing them completely with double distilled water and drying them before use. On stirring hot plate (Model 210T, Thermo Fisher Scientific Inc., USA) dilute 1 ml of 3 mM $HAuCl_4$ solution with 9 ml double distilled water and heat at 100 °C with vigorous stirring (500 rpm) until it begins to boil. Once boiled, add 1 ml of 1% trisodium citrate solution and continue heating and stirring until the color changed into a ruby red color which is considered as an indication of AuNPs formation of particle size less than 100 nm.[21] Here, stop heating and continue stirring until the solution cools down and reaches room temperature. The gold nanoparticles were re-dispersed after separation by a centrifuge in deionized water and this solution kept at 4 °C for further uses.

Mex-AuNPs were prepared by magnetic stirring of AuNPs with a methotrexate solution (1 mg / ml) for pre-set time periods of up to 90 min to determine the optimal stirring time to obtain maximum methotrexate loading efficiency%. The Mex-AuNPs solution was centrifuged and then re-dispersed in deionized water for following characterization studies.

Characterization of Mex-AuNPs

Determination of Loading Capacity and Methotrexate Loading Efficiency%

The prepared Mex-AuNPs was centrifuged at 12,000 rpm for 35 min. The free Mex present in the supernatant was determined by measuring its UV absorbance at 303 nm[22] using (Shimadzu UV 1700 spectrophotometer, Kyoto, Japan). The loading capacity and loading efficiency percent of methotrexate (Mex) were determined according the following equations[23]:

$$\text{Loading Capacity of Mex (mg/mg)} = (M_{Initial} - M_{Free}) / M_{Carrier}$$
$$\text{Loading Efficiency of Mex (\%)} = ((M_{Intial} - M_{Free}) / M_{Intial}) \text{ X } 100$$

Where $M_{Initial}$ and M_{Free} are the initial Mex content and free Mex content in supernatant, respectively and $M_{Carrier}$ is the weight of AuNPs.

UV-Visible Spectroscopy of Mex-AuNPs

The Mex-AuNPs was investigated by UV–visible Spectroscopy to confirm its production and determine the wavelength of the maximum absorption (λ_{max})[24]. It was re-investigated after 3 months of storage at room temperature to estimate the possible of change in λ_{max}.

Determination Particle Eize (PS), Zeta Potential (ZP) and Polydispersity Index (PDI) of Mex-AuNPs

The Zetasizer Nano ZS-90 instrument (Malvern Instruments, Worcestershire, UK) was used to determine PS, PDI and ZP for Mex-AuNPs; it examines light scattering fluctuations due to Brownian motion of particles.[25] The measurement was performed by suitability dilution with a 90 ° scattering angle at 25 ± 0.5 °C.

Morphological Examination

Transmission Electron Microscopy (TEM) (JEOL, JEM-100CX, Tokyo, Japan) was used to determine the morphology and core size of Mex-AuNPs. A drop of Mex-AuNPs dispersion was settled on a copper grid and left for dry until thin film formation. The film was stained and examined by TEM at 200 kV and magnification power of x100,000.[26]

In Vitro *Release of Mex from Mex-AuNPs*

In vitro Mex release from Mex-AuNPs was studied using cellulose acetate membrane diffusion cell in triplicate, at temperature 37 ± 0.5°C, 50 rpm shaker water bath, in 50 ml of different release media of phosphate buffer (pH 5 or pH 7.4) for comparison of different pH effect.[27] The dispersed Mex-AuNPs containing 1 mg of Mex was placed in tube with a Spectra Por© semi-permeable membrane on both sides and then immersed in the release medium. Samples (3 ml) of the release medium were withdrawn at pre-set time intervals (0.25–8 h) and were replaced immediately by an equal volume of fresh release medium to preserve a constant volume.[28] Samples were analyzed using UV-visible spectrophotometer at λ_{max} 303 nm. The cumulative drug release percentages (mean ± *S*.D.) were calculated and plotted against time to determine $Q_{0.5}$ h and Q_{8h}.

In Vitro *Cytotoxicity Betermination of Mex-AuNPs*

Cytotoxicity study is a useful initial step in determining the potential toxicity of Mex-AuNPs. The gold nanoparticles are safe to normal cells and not show a significant impact in cytotoxic effect[29] especially citrate gold nanoparticles[30] and spheres gold nanoparticles appears to be the safest one.[31] Hence, the gold nanoparticles can further be taken up to various biomedical applications. The proficiency of Mex-AuNPs in inhibiting the proliferation of human breast cancer cells MCF-7 was evaluated by a colorimetric MTT assay.[32] Human breast carcinoma cells (MCF-7) were cultured in DMEM media supplemented with L-glutamine (1%), gentamycin (1%) and FBS (10%) then incubated for 7 days under an atmosphere of 5% CO_2 at 37 °C.

Briefly, one hundred μl of MCF-7 was inoculated in a high density of 5×10^4 cells / well in a 96-well plate and incubated for 24 h. After that, the media were removed and Mex-AuNPs (1 mg/ml) were added at concentration of (0.02–50 μl/100 μl) to 36 wells by triplicate method. The positive control was designed by adding free methotrexate at similar concentrations to 36 wells. In another wells, the different volumes (0.02–50 μl/100 μl) have similar amount of AuNPs were added for testing their cytotoxicity, then 10 μl of 12 mM MTT stock solution (5 mg of MTT in 1 ml of phosphate buffer saline, PBS) to each well followed by incubation for 4 h under 5% CO_2 at 37 °C. One hundred μl of a solubilizing solution (DMSO) was added to each well with good mixing then incubated at 37 °C for 10 min. Cytotoxicity (loss of cell viability) on MCF-7 cells can be measured using MTT assay depending on the reduction of the yellow tetrazolium dye (MTT) by viable cells' enzymes to its insoluble purple formazan that can be used as an indication to amount of viable cells. DMSO was added to dissolve the insoluble purple formazan product into a colored solution so that the absorbance of this colored solution can be quantified by measuring spectrophotometrically at wavelength of 590 nm to determine the number of viable cells and the percentage of viability. The measured absorbances were used to calculate the percentage of cell viability (%) for each tested concentration relative to control according to the following equation:[33]

$$\text{The Cell Viability (\%)} = (A_{Test\ sample} / A_{Control}) \times 100$$

Where $A_{Test\ sample}$ and $A_{Control}$ are the absorbance of the test sample and the control, respectively.

The percentage of cell viability (%) was plotted *versus* Mex-AuNPs, free Mex and free AuNPs concentration, to get the survival curve. Graph pad Prism software (San Diego, CA. USA) was used for estimating the 50% inhibitory concentration (IC_{50}) from graphic plots of the dose response curve for each tested concentration.

Preparation of ^{99m}Tc-Methotrexate (^{99m}Tc-Mex)

Radiolabeling process was done at room temperature (~ 25 °C) by direct reduction method using sodium dithionite as a reducing agent. The factors (reducing agent concentration, Mex concentration, pH and reaction time) affecting the radiolabeling process were optimized to obtain the maximum radiolabeling efficiency. In a dry and clean 10 ml penicillin vial; different concentrations (0.5–50) mg/100 μl of the reducing agent, sodium dithionite ($Na_2S_2O_4$) and different concentrations (0.3–2) mg/100 μl of Mex were added to 100 μl of a fresh pertechnetate elute (7.2 MBq) at different reaction pH range from (3–10) adjusted by 0.1 N NaOH and 0.1 N HCl and the reaction volume was completed by deionized water to 500 μl at reaction times (5–60) min. Ascending paper chromatography was used for radiolabeling efficiency assessment using acetone as a mobile phase to determine free $^{99m}TcO_4^-$% and water: ethanol: ammonia mixture (5:2:1, *v:v:v*) to determine colloidal impurities (R-H $^{99m}TcO_2$)% using NaI (Tl) γ-ray scintillation counter (SPECTECH, ST450 SCA, USA) for measuring radioactivity. Radiochemical yield% an indication of the radiolabeling efficiency was calculated by the following equation:[18]

$$RCY\% = 100\% - \left(\text{Free}^{99m}TcO_4^-\% + \text{Colloid}(R - H^{99m}TcO_2)\%\right)$$

Preparation of ^{99m}Tc-Mex-AuNPs

The prepared ^{99m}Tc-Mex was filtered by 0.22 μm pore sterile filter (Millipore Co., Bedford, MA, USA) to remove colloidal radiolabeling impurities. ^{99m}Tc-Mex-AuNPs were prepared by magnetic stirring of AuNPs with a ^{99m}Tc-Mex solution for pre-set time periods of up to 90 min to determine the optimal stirring time to obtain maximum ^{99m}Tc-Mex loading efficiency%. The ^{99m}Tc-Mex-AuNPs solution was centrifuged and the radioactivity in precipitate (^{99m}Tc-Mex-AuNPs) and supernatant (free ^{99m}Tc-Mex) were measured by NaI (Tl) γ-ray scintillation counter. The ^{99m}Tc-Mex loading efficiency% was calculated according the following equation:[34]

$$^{99m}\text{Tc} - \text{Mex loadingefficiency}\% = \left(A/(A+B)\right) \times 100$$

Where A and B are the radioactivity in precipitate (^{99m}Tc-Mex-AuNPs) and supernatant (free ^{99m}Tc-Mex), respectively.

In Vitro *Stability of ^{99m}Tc-Mex-AuNPs in Mice Serum*

The *in vitro* stability of ^{99m}Tc-Mex-AuNPs was performed to evaluate its stability in physiological media, the feasibility of further *in-vivo* evaluations studies and confirming its suitability to be a physiologically stable nano-probe.[35] Exactly 100 μl of the ^{99m}Tc-Mex-AuNPs was incubated with 900 μl of normal mice serum for 24 h at 37 °C. The radiochemical yield% was measured by the previously described ascending paper chromatography method at 1, 2, 4, 8 and 24 h post-incubation.

In Vivo *Biodistribution Study*

Animals and Solid Tumor Induction

According to the ethical guidelines for animal care set by Egyptian Atomic Energy Authority (EAEA/2019/174), normal male Swiss albino mice (20–40 g), purchased from (National Cancer Institute, Egypt) were used for the biodistribution studies. First, for solid tumor induction 0.2 ml of Ehrlich Ascites solution (12.5×10^6 cells / ml) a parent

tumor line is injected into the muscle of the right thigh of mice, while the left thigh acted as a control.[36] Solid tumor begins to appear after about 10–15 days.

Biodistribution Assay

For the assessment of biological distribution and efficacy of tumor targeting of ^{99m}Tc-Mex-AuNPs, the mice were divided into three groups A, B and C (25 mice / group). Group A includes normal mice without solid tumor that were injected with ^{99m}Tc-Mex-AuNPs intravenously (I.V.), Groups B includes solid tumor bearing mice that were injected with ^{99m}Tc-Mex-AuNPs intravenously (I.V.) and Group C includes solid tumor bearing mice that were injected with ^{99m}Tc-Mex-AuNPs directly intratumor (I.T.). 100 μl of ^{99m}Tc-Mex-AuNPs (400 MBq) was injected intravenously (I.V.) in groups A and B while Group C was injected directly into solid tumor to evaluate biological distribution, targeting efficiency and target/non-target ratio (T/NT).

At pre-determined time intervals (10, 30, 60, 120 and 180 min) post injection (p.i.) 5 mice/time interval, the mice were anaesthetized by chloroform, sacrificed and weighed. Their organs, blood, muscle and tumor tissue in case of tumor bearing mice were removed, rinsed with saline and weighed in pre-weighed plastic vials. Radioactivity uptake for each organ as well as the background was detected using NaI (Tl) γ-ray scintillation counter and expressed as percent injected dose per gram of blood, organ and tumor (% ID/g ± SEM) using the following formula:[37]

$$\%\,\mathbf{ID/g\ of\ fluid/organ} = \frac{\mathbf{Radioactivity\ of\ tissue\ or\ fluid}}{\mathbf{Total\ injected\ radioactivity} \times \mathbf{weight\ of\ tissue\ or\ fluid(g)}} \times 100$$

The maximum drug concentrations in different organ and tumor (Cmax) were expressed in the maximum% ID/g of tumor.[38,39] The potentiality and tumor targeting efficiency were evaluated by the Tumor/Blood (T/B) ratio.[40,41]

Result and Discussion

Synthesis of Methotrexate Loaded Gold Nanoparticles (Mex-AuNPs)

Gold nanoparticles are mainly synthesized by various methods, including chemical, physical or biological methods.[42] Citrate-based method or Turkevich method one of the common chemical AuNPs synthesis technique includes reduction of Au $^{+3}$ in hydrogen tetrachloroaurate ($HAuCl_4$) to Au^0 (colloidal gold) using trisodium citrate ($Na_3C_6H_5O_7$) as a reducing and stabilizing agent in an aqueous solution and produces highly stable gold nanoparticles in size range of 15 –50 nm.[43, 44] The formation of gold nanoparticles of less than 100 nm was confirmed by changing in color to a ruby red color.[45] Mex-AuNPs were prepared by magnetic stirring of AuNPs with a methotrexate solution (1 mg / ml) for 30 min to obtain maximum methotrexate loading efficiency.

Characterization of Mex-AuNPs

Determination of Loading Capacity and Methotrexate Loading Efficiency %

The loading capacity and loading efficiency% of methotrexate in AuNPs were studied at different stirring time up to 90 min. Table 1 illustrated that the maximum loading capacity (0.093 ± 0.01 mg/mg) and loading efficiency% (93 ± 1.2%) of methotrexate in AuNPs were obtained at 30 min as an optimum stirring time. This could be as a result of the small particle size of AuNPs that facilitated drug loading.[46,47] Also, there is no change in the loading capacity and loading efficiency% by increasing the stirring time.

Table 1
The loading capacity and loading efficiency% of methotrexate in AuNPs at different stirring time.

Stirring time (min)	Free methotrexate concentration (mg/ml)	Loading capacity (mg/ mg)	Loading efficiency (%)
10	0.029 ± 0.01	0.071 ± 0.02	71 ± 1.01
20	0.017 ± 0.01	0.083 ± 0.01	83 ± 1.31
30	0.007 ± 0.00	0.093 ± 0.01	93 ± 1.2
60	0.007 ± 0.00	0.093 ± 0.01	93 ± 1.2
90	0.007 ± 0.00	0.093 ± 0.01	93 ± 1.2

UV–Visible Spectroscopy of Mex-AuNPs

The Mex-AuNPs were examined using UV–visible spectroscopy to determine their maximum absorption (λ_{max}) depending on the phenomenon of Localized Surface Plasmon Resonance (LSPR) and based on particle's size and shape exposed to light at specified wavelength. Liu et al., 2018 and Aryal et al., 2009[48, 49] illustrated that the spherical gold nanoparticles with size 10–22 nm, 50 and 100 nm showed maximum absorption at λ_{max}, 517–530 nm, 540 nm and 575 nm, respectively. Fig. 1 showed the strong absorption peak of Mex-AuNPs at λ_{max}, 525 nm with disappearance of the characteristic peaks of methotrexate at 303 nm.[50] This may be as result of the strong overlapping of AuNPs to methotrexate (LSPR).[51] In addition, there was no change in λ_{max} of Mex-AuNPs upon storage for 3 months at room temperature; confirming the stability.

Determination of Particle Size (PS), Zeta potential (ZP) and Polydispersity Index (PDI) of Mex-AuNPs

The particle size and zeta potential determination is very important to control the *in vitro* and *in vivo* behavior of Mex-AuNPs. The particle size of Mex-AuNPs was ≈ 20.3 nm and PDI value was in the acceptable range (< 0.5).[52] The zeta potential of Mex-AuNPs was −17.6 mV indicating considerable physical stability.[53]

Morphological Examination

Transmission Electron Microscopy (TEM) confirms the formation of a small spherical AuNPs varying in core sizes of (nearly) ≈ 10.3 nm as shown in Fig. 2.

In Vitro *Release of Mex from Mex-AuNPs*

The *in vitro* methotrexate release was studied to evaluate the stability of Mex-AuNPs in solution and it was done in phosphate buffer pH 5 and pH 7.4 to mimic the acidic tumor microenvironment and the physiological pH, respectively. Tumor cells exhibit lower acidity than that of normal cells which might lead to better tumor targeting and drug release from formulations.[54,55] As shown in Fig 3, the release profile of Mex from Mex-AuNPs illustrated higher drug release at pH 5, $Q_{0.5}$ h and Q_{8h} were 21.2 ± 1.5% and 92.9 ± 3.4%, respectively while, $Q_{0.5}$ h and Q_{8h} at pH 7.4 were 7.4 ± 1.25% and 18.8 ± 2.1%, respectively. The *in vitro* release profile of methotrexate from Mex-AuNPs at pH 5 exhibits biphasic drug release; initially relatively high release from the core shell followed by release from the core, allowing for sustained methotrexate release up to 8 h.[56] Consequently, methotrexate released from Mex-AuNPs highly accumulated in the tumor as a result of its acidic pH. As a result, it is possible to optimize the cytotoxic effects and improve tumor selective targeting using AuNPs drug delivery system for chemotherapeutics.[57,58]

In Vitro *Cytotoxicity of Mex-AuNPs*

The cytotoxic potential (Cell viability%) of Mex-AuNPs (1 mg/ml) in different concentrations (0.024–50 μl/100 μl) against MCF-7 breast cancer cells was investigated by MTT assay technique. As

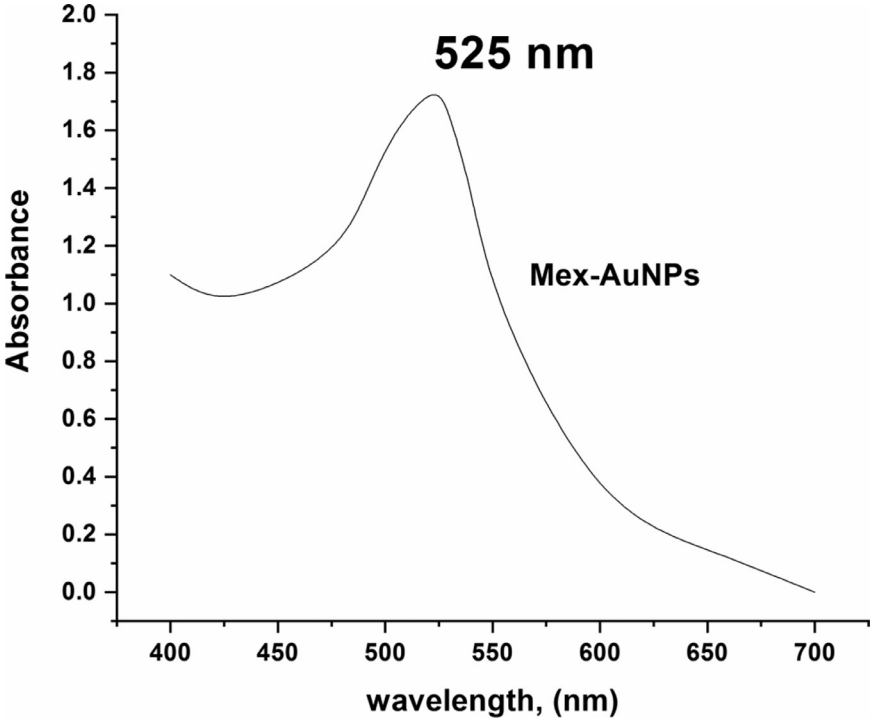

Figure 1. UV–visible spectroscopy of Mex-AuNPs.

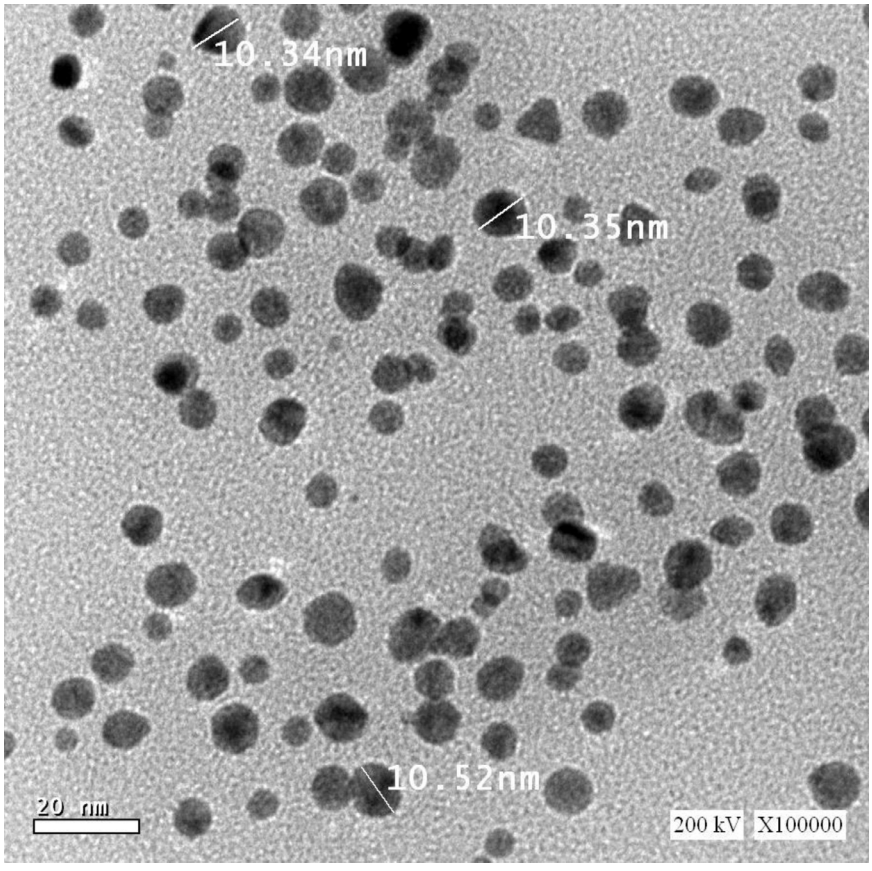

Figure 2. Transmission electron microscopy micrograph of Mex-AuNPs.

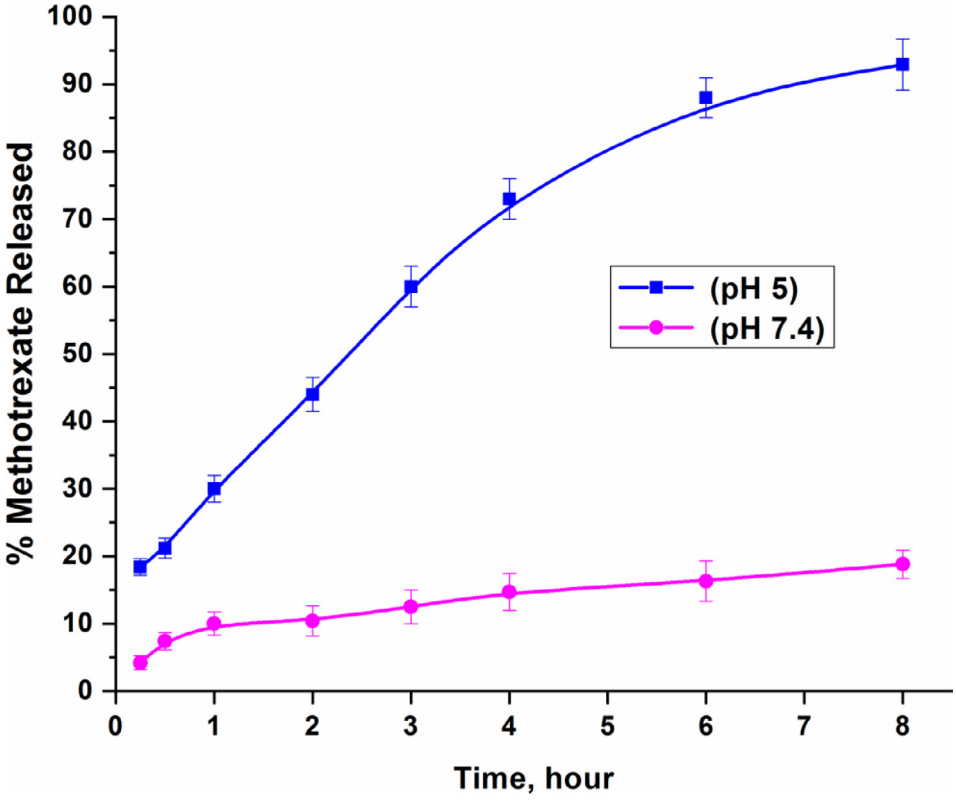

Figure 3. *In Vitro* methotrexate release profile from Mex-AuNPs at pH 5 and pH 7.4.

shown in Fig 4, the cell viability% decreased by increasing the concentration of Mex-AuNPs. The *in vitro* cytotoxicity results and Table 2 illustrated that the Mex-AuNPs showed higher anticancer activity with inhibitory concentration (IC_{50} = 0.098 ± 0.01 μl/100 μl) that three times lower than inhibitory concentration of free Mex (IC_{50} = 0.3 ± 0.04 μl/100 μl) and lower than the inhibitory concentration of free AuNPs (IC_{50}=0.8 ± 0.06 μl/100 μl). The high accumulation in tumor cell and the enhanced inhibitory activity of Mex-AuNPs with

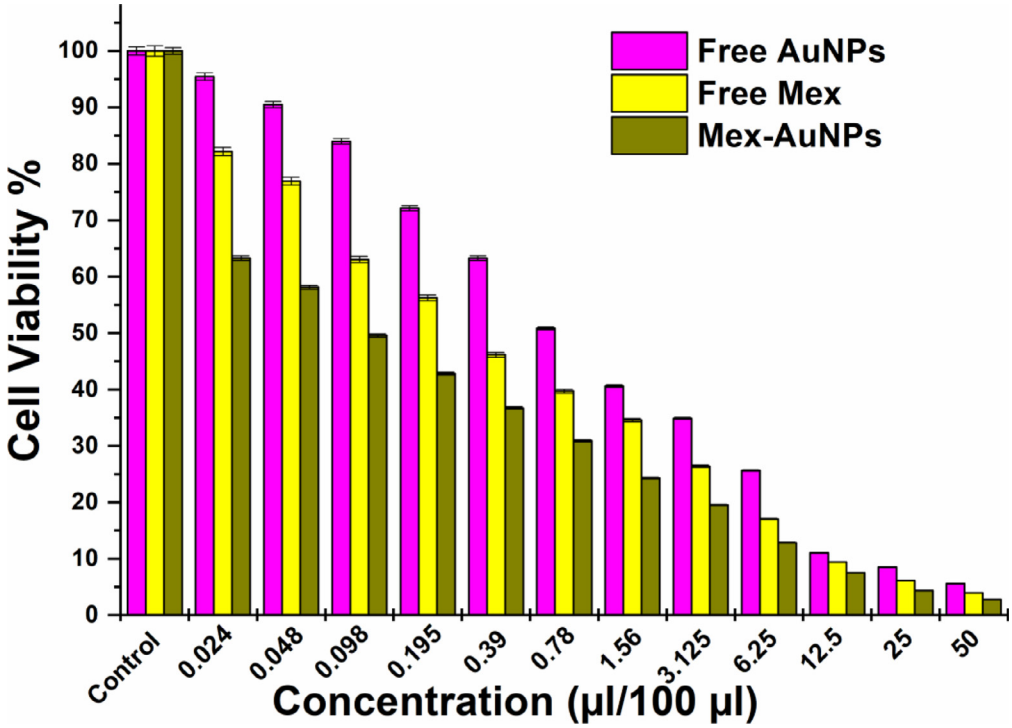

Figure 4. *In Vitro* cytotoxicity profiles of different concentration of Mex-AuNPs, free Mex and free AuNPs concentration against MCF-7 breast cancer cells, as investigated by MTT assay technique.

Table 2
Inhibitory concentration (IC_{50}) of Mex-AuNPs and free Mex solutions (1 mg/ml) against 100 μl of MCF-7 breast cancer cells (5×10^4 cells) as investigated by MTT assay technique.

	μl of solutions (mg/ml)	μg/ml	mM
Mex-AuNPs	0.098 ± 0.01	98 ± 10.1	0.22 ± 0.02
free Mex	0.3 ± 0.04	300 ± 40	0.66 ± 0.09

lower concentration (~ 1/3 of the free Mex concentration) may be due to the unique nanoscale particle size of gold nanoparticles that passively enter the cellular environment through fenestrations (~ 200 −780 nm) between the endothelial cells of defective architecture blood vessels, and retained due to the impaired lymphatic drainage this is called EPR effect.[59,60]

Preparation of ^{99m}Tc-Methotrexate (^{99m}Tc-Mex)

^{99m}Tc-Methotrexate was successfully prepared with maximum radiochemical yield (98.3 ± 1.09%) by direct reduction method using 100 μl of a fresh pertechnetate elute, 100 μl of Methotrexate solution (1 mg/100 μl) (Fig. 5A), 100 μl of sodium dithionite solution ($Na_2S_2O_4$) (30 mg/100 μl) (Fig. 5B), reaction pH 6 (Fig. 5C) and reaction time 15 min (Fig. 5D) at room temperature (~ 25 °C).

Preparation of ^{99m}Tc-Mex-AuNPs

The loading process of ^{99m}Tc-Mex with AuNPs depended on stirring time. The maximum loading efficiency% (93 ± 1.2%) of ^{99m}Tc-Methotrexat was obtained after a stirring time of 30 min similar to the stirring time required to obtain the maximum loading of methotrexate onto AuNPs.

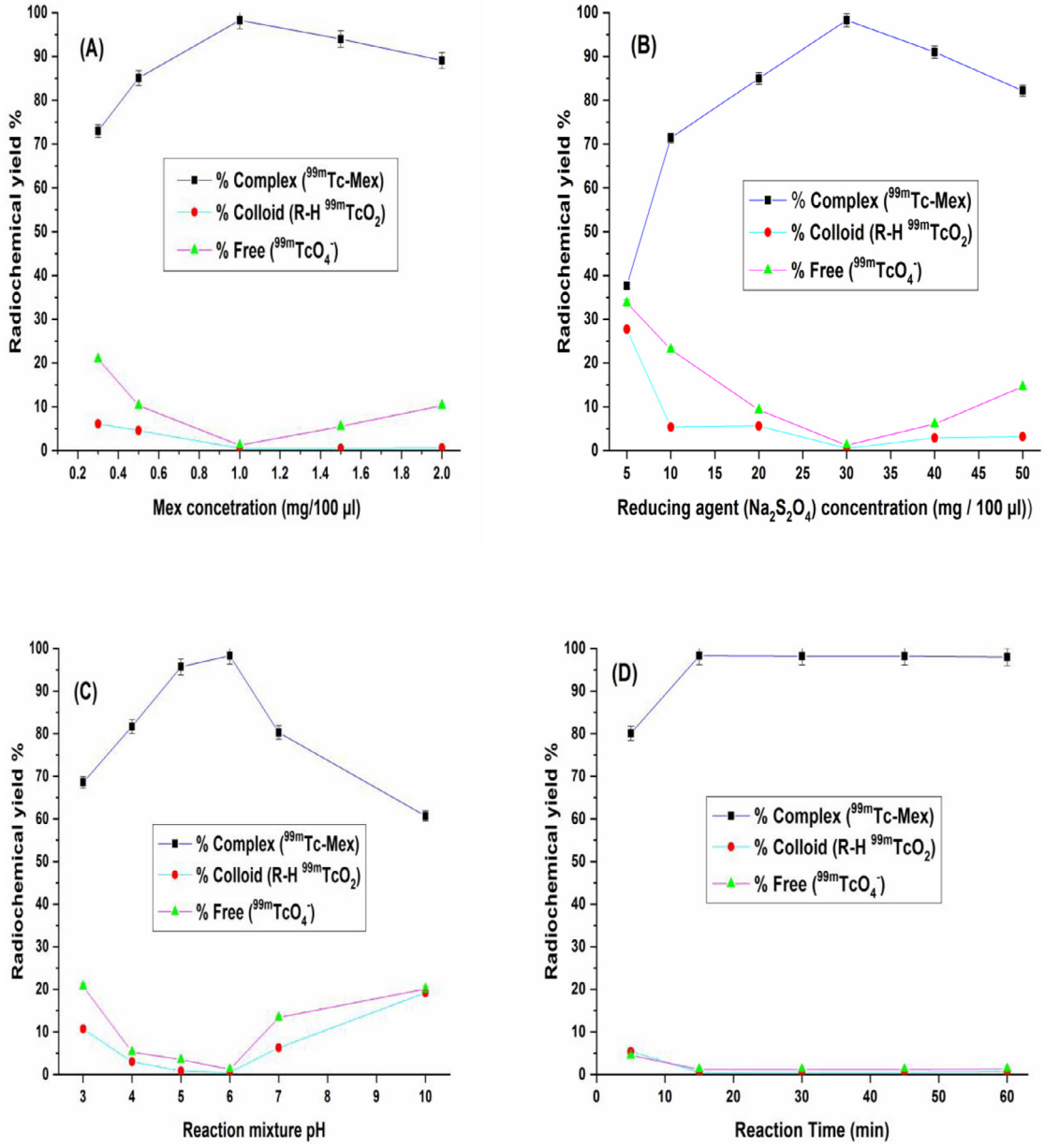

Figure 5. (A–D): Variation in the radiochemical yield% of ^{99m}Tc-Methotrexate (^{99m}Tc-Mex) complex as a function of (A) Mex concentration, (B) Reducing agent ($Na_2S_2O_4$) concentration, (C) Reaction mixture pH, (D) Reaction time.

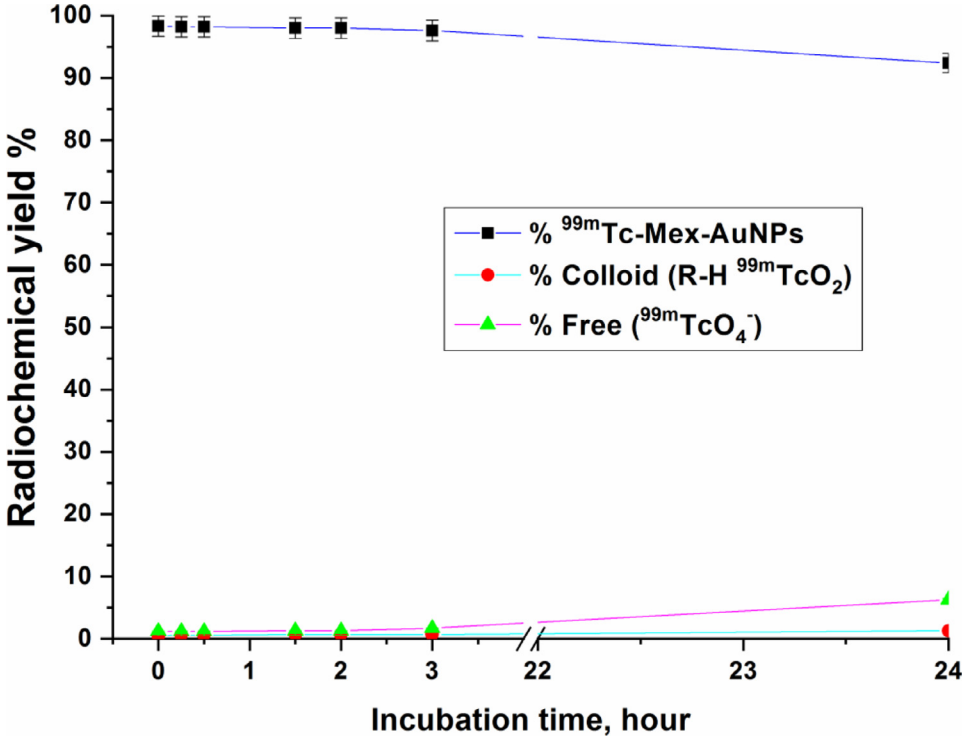

Figure 6. *In Vitro* stability of ^{99m}Tc-Mex-AuNPs in mice serum.

In Vitro *Stability of ^{99m}Tc-Mex-AuNPs in Mice Serum*

The *in vitro* stability of ^{99m}Tc-Mex-AuNPs was studied in normal mice serum. As shown in Fig. 6 the radiochemical yields estimated chromatographically, remained unchanged for 3 h post-incubation and slightly decreased by 6% only and still > 90% after 24 h incubation. This remarkable *in vitro* stability in a biological fluid definitely promises a convenient *in vivo* stability of the ^{99m}Tc-Mex-AuNPs.

In Vivo *Biodistribution Study*

The biodistribution study is very important to determine the pharmacokinetics of the newly nanoradiopharmaceuticals. The *in vivo* biodistribution of ^{99m}Tc-Mex-AuNPs was studied in three experimental mice groups A, B and C (25 mice / group). Group A included normal mice without solid tumor that were injected with ^{99m}Tc-Mex-AuNPs intravenously (I.V.) for determination of the ^{99m}Tc-Mex-AuNPs biodistribution pattern. Groups B and C included solid tumor bearing mice to study the accumulation of ^{99m}Tc-Mex-AuNPs in solid tumor following I.V. and direct intratumor (I.T.) injection, respectively. In A, B and C groups the% ID/g of different organs, blood and tumor were determined post injection at pre-set time intervals (10, 30, 60, 120 and 180 min) using 5 mice/time interval (Fig. 7, A–C). Group A showed the normal biodistribution with high accumulation of ^{99m}Tc-Mex-AuNPs in the liver (25.79 ± 0.36%ID/g) and spleen (23.27 ± 0.33%ID/g) at 120 min post intravenous injection (Fig. 7, A). This may be due to the accumulation of gold nanoparticles in reticuloendothelial organs (liver and spleen)[61] due to the nature of the leaky blood vessels of these organs and the phagocytic uptake by macrophages.[62,63] Fig. 7A indicates an increase in the blood concentration of ^{99m}Tc-Mex-AuNPs to 16 ± 0.18% ID / g at 30 min post intravenous injection in normal mice, and this may be due to small particle size whereas the particles with a diameter of 100 nm or less avoiding internalization with Mononuclear Phagocyte System (MPS) by longer circulation times in order to reduce clearance by macrophages.[64] Then, the nanoparticles are recognized by MPS with opsonization which consists of the binding of blood opsonins to nanoparticles' surface thus, inducing its phagocytosis and accumulation in the liver (Kuppfer cells). The liver acts as a reservoir toward nanoparticles conditioning their rapid first-phase disappearance from the blood.[65]

The biodistribution profile for group B in Fig. 7 B is revealed to lower accumulation of ^{99m}Tc-Mex-AuNPs in liver and spleen than group A. The blood concentration decreased gradually over time with increasing in tumor accumulation at 60 min post intravenous injection and this may be due to tumor accumulation of ^{99m}Tc-Mex-AuNPs because active tumor targeting of methotrexate (a folic acid analogue) and passive targeting of small sized gold nanoparticles due to high enhanced permeability and retention (EPR) effects that facilitate penetration and accumulation of ^{99m}Tc-Mex-AuNPs at the tumor.[66,67] Fig. 7 C showed the importance of intratumoral injection of ^{99m}Tc-Mex-AuNPs in reducing its side effects due to the minimal accumulation within the organs.

The comparative tumor uptake of ^{99m}Tc-Mex-AuNPs between I.T. and I.V. injection for group B and group C, respectively in Fig. 7 D showed the dramatic differences in tumor accumulations where the maximum tumor uptake of ^{99m}Tc-Mex-AuNPs in group B was 20 ± 0.42%ID/g at 60 min post I.V. injection while the group C achieved highest tumor uptake (93 ± 0.39%ID/g) at 10 min post direct I.T. injection in solid tumor and retained with high tumor uptake (79 ± 0.65%ID/g) up to 60 min post I.T. injection before escaping into blood stream.

It is important to evaluate the target (solid tumor in the right thigh) to non-target (the muscle in the left thigh) (T/NT) ratios of ^{99m}Tc-Mex-AuNPs as revealed in Fig. 8. It is demonstrated that promising results were obtained throughout all the experimental time points. The maximum T/NT ratios of 12.5 ± 0.21 and 58.1 ± 0.91were achieved at 60 and 10 min post I.V. and I.T. injection, respectively. The potentiality of a new nanoradiopharmaceutical depends on the Tumor/Blood (T/B) ratio that must be higher than one. The ^{99m}Tc-Mex-AuNPs showed T/B ratio > 1 at all-time post I.T. delivery and at

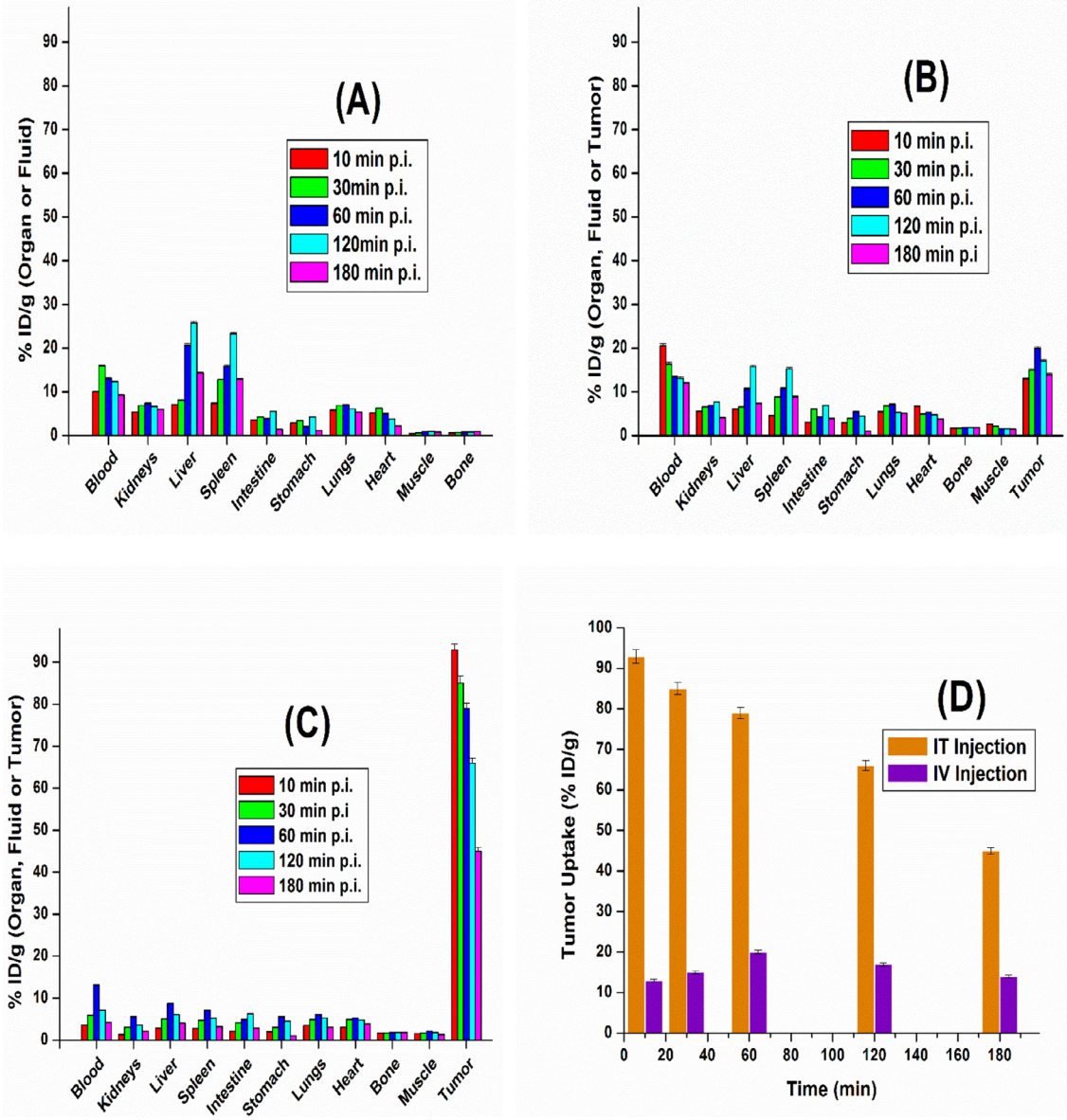

Figure 7. (A–D): The comparative *in vivo* biodistribution and tumor uptake of ^{99m}Tc-Mex-AuNPs (% ID/g ± SEM, n = 5) in normal and tumor bearing mice at pre-determined time intervals post-injection A (Intravenous injected normal mice), B (Intravenous injected tumor bearing mice), C (Intratumoral injected tumor bearing mice) and D (The comparative Tumor uptake of ^{99m}Tc-Mex-AuNPs post Intratumoral and Intravenous injection).

60, 120 and 180 min post I.V. injection (Table 3) with drug targeting efficiency percent (DTE%) higher than 100% at all-time points. Consequently, ^{99m}Tc-Mex-AuNPs can be considered new potential nanoradiopharmaceutical in tumor diagnosis.

Conclusion

Development of specialized nanoradiopharmaceuticals for use in tumor diagnosis and treatment has become an urgent necessity. The AuNPs was synthesized by a modified Turkevich technique using trisodium citrate as a reducing and stabilizing agent. The Mex-AuNPs successfully prepared in small spherical particle size (20.3 nm), PDI (< 0.5) and a zeta potential (−17.6 mV) with loading efficiency% (93 ± 1.2%) of methotrexate at 30 min as an optimum stirring time and showed strong absorption peak for Mex-AuNPs at λ_{max}, 525 nm. The Mex-AuNPs showed *in vitro* higher release percent (Q_{8h}; 92.9 ± 3.4%) of methotrexate at pH 5 than physiological pH 7.4. The Mex-AuNPs presented high anticancer activity against MCF-7 breast cancer cells with inhibitory concentration (IC_{50} = 0.098 μl/100 μl) that three times lower than inhibitory concentration of free Mex. The methotrexate was radiolabeled by ^{99m}Tc in maximum radiochemical yield% ≈ 98.3 ± 1.09% using direct labeling process, and high efficiently loaded (loading efficiency ≈ 93%) to prepare ^{99m}Tc-Mex-AuNPs. The preclinical biodistribution study results in solid tumor bearing mice showed the highest tumor uptake (20 ± 0.42%ID/g) at 60 min post I.V. injection and (93 ± 0.39%ID/g) at 10 min post direct I. T. injection in solid tumor in addition the highest T/NT ratio (58.1 ± 0.91 at 10 min post I.T. injection) and T/B ratio > 1 at all-time post I.T. injection. This superior tumor targeting and selectivity of ^{99m}Tc-Mex-AuNPs and also its enhanced cytotoxicity qualify it to be a new theranostic nano-radiopharmaceutical with dual use in diagnosis and treatment of tumors.

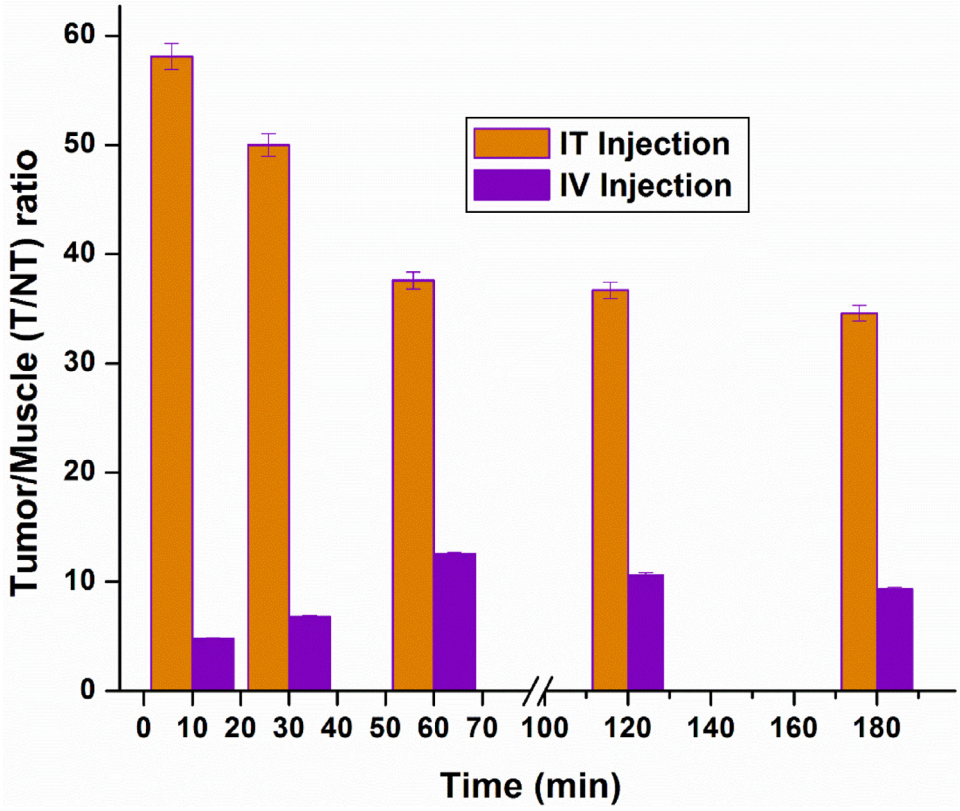

Figure 8. Target to non target (T/NT) ratios of ^{99m}Tc-Mex-AuNPs as a function of time following Intratumoral and Intravenous injection.

Table 3
Tumor to blood (T/B) ratios of ^{99m}Tc-Mex-AuNPs as a function of time following Intratumoral (IT) and Intravenous (IV) injection.

Time (min)	^{99m}Tc-Mex-AuNPs	
	T/B_{IT}	T/B_{IV}
10	25.8 ± 0.2	0.63 ± 0.03
30	14.4 ± 0.1	0.91 ± 0.01
60	6.07 ± 0.09	1.49 ± 0.02
120	9.3 ± 0.09	1.28 ± 0.02
180	8.2 ± 0.08	1.17 ± 0.01

CRediT Authorship Contribution Statement

DM El-Safoury: Investigation, Methodology, Software, Formal analysis, Writing – original draft. **AB Ibrahim:** Conceptualization, Validation, Resources, Software, Writing – review & editing. **DA El-Setouhy:** Resources, Writing – review & editing, Supervision. **OM Khowessah:** Conceptualization, Supervision. **MA Motaleb:** Writing – review & editing, Supervision. **Tamer M. Sakr:** Conceptualization, Validation, Resources, Writing – review & editing, Project administration, Funding acquisition, Supervision.

Declaration of Competing Interest

The authors declare that they have no known competing financial interests or personal relationships that could have appeared to influence the work reported in this paper.

Acknowledgments

Associate Prof. Tamer M. Sakr expresses his grateful appreciation and thanks for International Atomic Energy Authority (IAEA), Austria for the international collaboration and funding this work under CRP No. F22064.

References

1. American Cancer Society. Cancer facts and figures. *Genes Dev*. 2017;21:2525–2538.
2. Lee S, Chon H, Lee M, et al. Surface-enhanced Raman scattering imaging of HER_2 cancer markers overexpressed in single MCF_7 cells using antibody conjugated hollow gold nanospheres. *Biosens Bioelectron*. 2009;24(7):2260–2263.
3. Amadori D, Silvestrini R, Lena M, et al. Ran-domized phase III trial of adjuvant epirubicin followed by cyclophosphamide,methotrexate, and 5-fluorouracil (CMF) *versus* CMF followed by epirubicin in patients with node-negative or 1–3 node-positive rapidly proliferating breast cancer. *Breast Cancer Res Treat*. 2011;125 (3):775–784.
4. Neradil J, Pavlasova G, Veselska R. New mechanisms for an old drug; DHFR- and non-DHFR-mediated effects of methotrexate in cancer cells. *Klin Onkol*. 2012;25 (2):2587–2592.
5. Choi G, Kim TH, Oh JM, Choy JH. Emerging nanomaterials with advanced drug delivery functions; focused on methotrexate delivery. *Coord Chem Rev*. 2018;359:32–51.
6. Raffa RB, Duong PV, Finney J, et al. Is 'chemofog'/'chemo-brain' caused by cancer chemotherapy? *J. Clin Pharm Ther*. 2006;31(2):129–138.
7. Tran NTT, Wang TH, Lin CY, Tai Y. Synthesis of methotrexate-conjugated gold nanoparticles with enhanced cancer therapeutic effect. *Biochem Eng J*. 2013;78:175–180.
8. Khodadadei F, Safarian S, Ghanbari N. Methotrexate-loaded nitrogen-doped graphene quantum dots nanocarriers as an efficient anticancer drug delivery system. *Mater Sci Eng C Mater Biol Appl*. 2017;79:280–285.
9. Ting G, Chang CH, Wang HE. Cancer nanotargeted radiopharmaceuticals for tumor imaging and therapy. *Anticancer Res*. 2009;29:4107–4118.
10. Débora BV, Lionel FG. Advances in the use of nanocarriers for cancer diagnosis and treatment. *Einstein*. 2016;14(1):99–103. Sao Paulo.
11. Din FU, Aman W, Ullah I, et al. Effective use of nanocarriers as drug delivery systems for the treatment of selected tumors. *Int J Nanomed*. 2017;12:7291–7309.
12. Xie H, Gu S, Zhang J, Hu Q, Yu X, Kong J. Novel PEI-AuNPs-Mn III PPIX nanocomposite with enhanced peroxidase-like catalytic activity in aqueous media. *C R Chim*. 2018;21(2):104–111.
13. Wang J, Fang X, Cui X, et al. A highly sensitive colorimetric probe for Cd^{2+}, Hg^{2+} and ascorbic acid determination based on trithiocyanuric acid-AuNPs. *Talanta*. 2018;188:266–272.

14. Álvarez-González B, Rozalen M, Fernández-Perales M, Álvarez MA, Sánchez-Polo M. Methotrexate gold nanocarriers: loading and release study: its activity in colon and lung cancer cells. *Molecules*. 2020;25(24):6049.
15. Chen YH, Tsai CY, Huang PY, et al. Methotrexate conjugated to gold nanoparticles inhibits tumor growth in a syngeneic lung tumor model. *Mol Pharm*. 2007;4 (5):713–722.
16. Su N, Dang Y, Liang G, Liu G. Iodine-labeled cRGD-gold nanoparticles as tumor-targeted radiosensitizer and imaging agent. *Nanoscale Res Lett*. 2015;10(1):160.
17. Same S, Aghanejad A, Akbari NS, Barar J, Omidi Y. Radiolabeled theranostics: magnetic and gold nanoparticles. *Bioimpacts*. 2016;6(3):169–181.
18. Sakr TM, Khowessah OM, Motaleb MA, El-Bary AA, El-Kolaly MT, Swidan MM. I-131 doping of silver nanoparticles platform for tumor theranosis guided drug delivery. *Eur J Pharm Sci*. 2018;122:239–245.
19. Kettemann F, Birnbaum A, Witte S, et al. Missing piece of the mechanism of the turkevich method: the critical role of citrate protonation. *Chem Mater*. 2016;28 (11):4072–4081.
20. Turkevich J, Stevenson PC, Hillier J. A Study of the nucleation and growth processes in the synthesis of colloidal gold. *Discuss Faraday Soc*. 1951;11:55–75.
21. Hu M, Chen JY, Li ZY, et al. Gold nanostructures: engineering their plasmonic properties for biomedical applications. *Chem Soc Rev*. 2006;35(11):1084–1094.
22. Rozalen M, Sánchez-Polo M, Fernández-Perales M, Widmann TJ, Rivera-Utrilla J. Synthesis of controlled-size silver nanoparticles for the administration of methotrexate drug and its activity in colon and lung cancer cells. *RSC Adv*. 2018;10 (18):10646–10660.
23. Vinod LG, Prafulla BC, Neela MB, Manish SB. Characterization of pharmaceutical nanocarriers: *in vitro* and *in vivo* studies. *Nanomaterials for drug delivery and therapy*. 2. Amsterdam, Netherlands: Elsevier; 2019:33–58.
24. Bhumkar DR, Joshi HM, Sastry M, Pokharkar VB. Chitosan reduced gold nanoparticles as novel carriers for transmucosal delivery of insulin. *Pharm Res*. 2007;24 (8):1415–1426.
25. Scognamiglio I, De Stefano D, Campani V, et al. Nanocarriers for topical administration of resveratrol: a comparative study. *Int J Pharm*. 2013;440(2):179–187.
26. Fahmy AM, El-Setouhy DA, Ibrahim AB, Habib BA, Tayel SA, Bayoumi NA. Penetration enhancer-containing spanlastics (PECSs) for transdermal delivery of haloperidol: *in vitro* characterization, *ex vivo* permeation and *in vivo* biodistribution studies". *Drug Deliv*. 2018;25(1):12–22.
27. El-Ghareb WI, Swidan MM, Ibrahim IT, Abd El-Bary A, Tadros MI, Sakr TM. ^{99m}Tc-doxorubicin-loaded gallic acid-gold nanoparticles (^{99m}Tc-DOX-loaded GA-Au NPs) as a multifunctional theranostic agent. *Int J Pharm*. 2020;586: 119514.
28. Shamma RN, Elsayed I. Transfersomal lyophilized gel of buspirone HCl: formulation, evaluation and statistical optimization. *J Liposome Res*. 2013;23(3):244–254.
29. Jeyarani S, Vinita NM, Puja P, et al. Biomimetic gold nanoparticles for its cytotoxicity and biocompatibility evidenced by fluorescence-based assays in cancer (MDA-MB-231) and non-cancerous (HEK-293) cells. *J Photochem Photobiol B Biol*. 2020. https://doi.org/10.1016/j.jphotobiol.2019.111715.
30. Steckiewicz KP, Barcinska E, Malankowska A, et al. Impact of gold nanoparticles shape on their cytotoxicity against human osteoblast and osteosarcoma in *in vitro* model. evaluation of the safety of use and anti-cancer potential. *J Mater Sci Mater Med*. 2019;30(2):22.
31. Martínez-Torres AC, Zarate-Triviño DG, Lorenzo-Anota HY, Ávila-Ávila A, Rodríguez-Abrego C, Rodríguez-Padilla C. Chitosan gold nanoparticles induce cell death in HeLa and MCF-7 cells through reactive oxygen species production. *Int J Nanomedicine*. 2018;13:3235–3250.
32. Abdulaziz M, Al-mahallawi Ahmed RF, Wessam HA. Enhanced permeation of methotrexate via loading into ultra-permeable niosomal vesicles: fabrication, statistical optimization, *Ex Vivo* studies, and *In Vivo* skin deposition and tolerability. *AAPS Pharm Sci Tech*. 2019;20:171–181.
33. Peng M, Li H, Luo Z, et al. Dextran-coated superparamagnetic nanoparticles as potential cancer drug carriers *in vivo*. *Nanoscale*. 2015;7(25):11155–11162.
34. Sakr TM, El-Safoury DM, Awad GA, Motaleb MA. Biodistribution of ^{99m}Tc-sunitinib as a potential radiotracer for tumor hypoxia imaging. *J Labelled Comp Radiopharm*. 2013 a;56(8):392–395.
35. Swidan MM, Sakr TM, Motaleb MA, Abd El-Bary AA, El-Kolaly MT. Radioiodinated acebutolol as a new highly selective radiotracer for myocardial perfusion imaging. *J Labelled Comp Radiopharm*. 2014;57(10):593–599.
36. Ibrahim AB, Salem AM, Fasih TW, Brown A, Sakr TM. Radioiodinated doxorubicin as a new tumor imaging model: preparation, biological evaluation, docking and molecular dynamics. *J Radioanal Nucl Chem*. 2018;317(3):1243–1252.
37. Shamsel-Din HA, Ibrahim AB. A novel radiolabeled indole derivative as solid tumor imaging agent: in silico and preclinical pharmacological study. *J Radioanal Nucl Chem*. 2017;314(3):2263–2269.
38. El-Setouhy DA, Ibrahim AB, Amin MM, Khowessah OM, Elzanfaly ES. Intranasal haloperidol-loaded miniemulsions for brain targeting: evaluation of locomotor suppression and in-vivo biodistribution. *Eur J Pharm Sci*. 2016;92:244–254.
39. Chow HS, Chen Z, Matsuura GT. Direct transport of cocaine from the nasal cavity to the brain following intranasal cocaine administration in rats. *J Pharm Sci*. 1999;88 (8):754–758.
40. Yadav S, Gattacceca F, Panicucci R, Amiji MM. Comparative biodistribution and pharmacokinetic analysis of cyclosporine-a in the brain upon intranasal or intravenous administration in an oil-in-water nanoemulsion formulation. *Mol Pharm*. 2015;12(5):1523–1533.
41. Kozlovskaya L, Abou-Kaoud M, Stepensky D. Quantitative analysis of drug delivery to the brain via nasal route. *J Control Release*. 2014;189:133–140.
42. Hossen S, Hossain MK, Basher MK, Mia MNH, Rahman MT, Uddin MJ. Smart nanocarrier-based drug delivery systems for cancer therapy and toxicity studies. a review. *J Adv Res*. 2018;15:1–18.
43. Verma HN, Singh P, Chavan RM. Gold nanoparticle: synthesis and characterization. *Vet World*. 2014;7(2):72–77.
44. Dong J, Carpinone PL, Pyrgiotakis G, Demokritou P, Moudgil BM. Synthesis of precision gold nanoparticles using turkevich method. *Kona Powder Sci Technol Jpn*. 2020;37:224–232.
45. Khan S, Alam F, Azam A, Khan AU. Gold nanoparticles enhance methylene blue-induced photodynamic therapy: a novel therapeutic approach to inhibit candida albicans biofilm. *Int J Nanomed*. 2012;7:3245–3257.
46. Raghunand N, Mahoney BP, Gillies RJ. Tumor acidity, ion trapping and chemotherapeutics: II. pH-dependent partition coefficients predict importance of ion trapping on pharmacokinetics of weakly basic chemotherapeutic agents. *Biochem Pharmacol*. 2003;66(7):1219–1229.
47. Curry D, Cameron A, MacDonald B, et al. Adsorption of doxorubicin on citrate-capped gold nanoparticles: insights into engineering potent chemotherapeutic delivery systems. *Nanoscale*. 2015;7(46):19611–19619.
48. Liu Y, Crawford BM, Vo-Dinh T. Gold nanoparticles-mediated photothermal therapy and immunotherapy. *Immunotherapy*. 2018;10(13):1175–1188.
49. Aryal S, Grailer JJ, Pilla S, Steeber DA, Gong S. Doxorubicin conjugated gold nanoparticles as water-soluble and pH-responsive anticancer drug nanocarriers. *J Mater Chem*. 2009;19(42):7879–7884.
50. Ranjbar-Navazi Z, Eskandani M, Johari-Ahar M, et al. Doxorubicin-conjugated D-glucosamine-and folate-bi-functionalised InP/ZnS quantum dots for cancer cells imaging and therapy. *J Drug Target*. 2018;26(3):267–277.
51. Chaudhary A, Dwivedi C, Gupta A, Nandi CK. One pot synthesis of doxorubicin loaded gold nanoparticles for sustained drug release. *RSC Adv*. 2015;5 (118):97330–97334.
52. Cho HJ, Park JK, Yoon IS, Kim DD. Surface-modified solid lipid nanoparticles for oral delivery of docetaxel: enhanced intestinal absorption and lymphatic uptake. *Int J Nanomed*. 2014;9:495–504.
53. Honary S, Zahir F. Effect of zeta potential on the properties of nano-drug delivery systems-a review (Part 2). *Trop J Pharm Res*. 2013;12(2):265–273.
54. Cheng R, Meng F, Deng C, Klok HA, Zhong Z. Dual and multi-stimuli responsive polymeric nanoparticles for programmed site-specific drug delivery. *Biomaterials*. 2013;34(14):3647–3657.
55. Yang Y, Lin Y, Di D, et al. Gold nanoparticle-gated mesoporous silica as redox-triggered drug delivery for chemo-photothermal synergistic therapy. *J Colloid Interface Sci*. 2017;508:323–331.
56. Torchilin V, Amiji MM. Polymeric micelles as versatile carriers for drugs and nucleic acids delivery. *handbook of materials for nanomedicine*. Danvers (MA): Pan Stanford Publishing; 2010:190–210.
57. Gerweck LE, Vijayappa S, Kozin S. Tumor pH controls the *in vivo* efficacy of weak acid and base chemotherapeutics. *Mol Cancer Ther*. 2006;5(5):1275–1279.
58. Kelly KL, Coronado E, Zhao LL, Schatz GC. The optical properties of metal nanoparticles: the influence of size, shape, and dielectric environment. *J Phys Chem B*. 2003;107(3):668–677.
59. Hobbs SK, Monsky WL, Yuan F, et al. Regulation of transport pathways in tumor vessels: role of tumor type and microenvironment. *Proc Natl Acad Sci USA*. 1998;95 (8):4607–4612.
60. Dreaden EC, Austin LA, Mackey MA, El-Sayed MA. Size matters: gold nanoparticles in targeted cancer drug delivery. *Ther Deliv*. 2012;3(4):457–478.
61. Singh P, Pandit S, Mokkapati VRSS, Garg A, Ravikumar V, Mijakovic I. Gold nanoparticles in diagnostics and therapeutics for human cancer. *Int J Mol Sci*. 2018;19 (7):1979.
62. Nie S. Understanding and overcoming major barriers in cancer nanomedicine. *Nanomedicine*. 2010;5(4):523–528.
63. Mondal N, Halder KK, Kamila MM, et al. Preparation, characterization, and biodistribution of letrozole loaded PLGA nanoparticles in ehrlich ascites tumor bearing mice. *IntJ Pharm*. 2010;397(1–2):194–200.
64. Choi HS, Liu W, Misra P, et al. Renal clearance of quantum dots. *Nat Biotechnol*. 2007;25(10):1165–1170. (2007).
65. Owens DE, Peppas NA. Opsonization, biodistribution, and pharmcokinetics of polymeric nanoparticles. *Int J Pharm*. 2006;307(1):93–102.
66. Kobayashi H, Watanabe R, Choyke PL. Improving conventional enhanced permeability and retention (EPR) effects; what is the appropriate target?.. *Theranostic*. 2013;4(1):81–89.
67. Ruttala HB, Ramasamy T, Madeshwaran T, et al. Emerging potential of stimulus-responsive nanosized anticancer drug delivery systems for systemic applications. *Arch Pharm Res*. 2018;41(2):111–129.